

Poisson-Nernst-Planck-Fermi Theory for Ion Channels

Jinn-Liang Liu

*Department of Applied Mathematics, National Hsinchu University of Education,
Hsinchu 300, Taiwan. E-mail: jinnliu@mail.nhcue.edu.tw*

Bob Eisenberg

*Department of Molecular Biophysics and Physiology, Rush University,
Chicago, IL 60612 USA. E-mail: beisenbe@rush.edu**

(Dated: June 4, 2022)

Abstract. A Poisson-Nernst-Planck-Fermi (PNPF) theory is developed for studying ionic transport through biological ion channels. Our goal is to deal with the finite size of particle using a Fermi like distribution without calculating the forces between the particles, because they are both expensive and tricky to compute. We include the steric effect of ions and water molecules with nonuniform sizes and interstitial voids, the correlation effect of crowded ions with different valences, and the screening effect of water molecules in an inhomogeneous aqueous electrolyte. Including the finite volume of water and the voids between particles is an important new part of the theory presented here. Fermi like distributions of all particle species are derived from the volume exclusion of classical particles. Volume exclusion and the resulting saturation phenomena are especially important to describe the binding and permeation mechanisms of ions in a narrow channel pore. The Gibbs free energy of the Fermi distribution reduces to that of a Boltzmann distribution when these effects are not considered. The classical Gibbs entropy is extended to a new entropy form — called Gibbs-Fermi entropy — that describes mixing configurations of all finite size particles and voids in a thermodynamic system where microstates do not have equal probabilities. The PNPF model describes the dynamic flow of ions, water molecules, as well as voids with electric fields and protein charges. The model also provides a quantitative mean-field description of the charge/space competition mechanism of particles within the highly charged and crowded channel pore. The PNPF results are in good accord with experimental currents recorded in a 10^8 -fold range of Ca^{2+} concentrations. The results illustrate the anomalous mole fraction effect, a signature of L-type calcium channels. Moreover, numerical results concerning water density, dielectric permittivity, void volume, and steric energy provide useful details to study a variety of physical mechanisms ranging from binding, to permeation, blocking, flexibility, and charge/space competition of the channel.

1. INTRODUCTION

Biological functions of proteins depend on the details of the mixtures of ionic solutions found outside and inside cells. Trace concentrations ($< 10^{-6}$ M) of calcium ions (Ca^{2+}) and other signaling molecules provide physiological control of many biological pathways and proteins inside cells [1]. For example, voltage-gated calcium (Ca_V) channels exhibit the

*A different version of this paper was published in J. Chem. Phys. 141 (2014) 22D532.

anomalous mole fraction effect that effectively blocks abundant monovalent cations by a trace concentration of Ca^{2+} ions [2–4]. The fundamental mechanism of the calcium channel is of great technological and biological interest [5, 6]. Multiscale analysis seems necessary since calibrated all atom simulations of trace concentrations of ions in physiological solutions are not likely to be available in the near future.

Interactions between diffusion and migration in the electric field are central to the biologists’ view of channels [7, 8]. Following the drift-diffusion (DD) model in semiconductors, Eisenberg et al. [9–11] have proposed the Poisson-Nernst-Planck (PNP) model to calculate rather than assume [7, 8] the electric field and then the ionic current in biological ion channels. Interactions of ions and flows in narrow channels, and saturation in binding sites are also central to the biologists’ view of channels [7, 8]. It has been difficult to combine the two views — computed electric fields in channels showing interactions and saturation — because charges in PNP (and quasiparticles in DD) are points with no diameter and so cannot saturate the aqueous channel [1] the way real ions do. Recently, the saturation of spheres of any size has been described by a Fermi like distribution derived in [12] from the configuration entropy of mixtures of ions of any diameter and composition. The steric effect has been shown to be very important to adequately describe equilibrium systems [12–14].

We extend the Poisson-Fermi model [12] in two important rather novel ways. We include the excluded volume of water molecules and the ‘empty space’ created by packing constraints and voids between particles. The equilibrium model is also generalized here to a nonequilibrium model called the Poisson-Nernst-Planck-Fermi (PNPF) model that can describe flow, including the steric effect of all particles, the correlation effect of ions and water molecules, the screening effect of water, as well as the charge/space mechanism in the channel pore at and away from equilibrium. This treatment unites diffusion and electric current, with interactions and binding in narrow channels.

Both discrete and continuum forms of Gibbs free energy of the electrolyte are developed in this paper. The Gibbs-Fermi free energy functional for the Fermi distribution is shown to reduce to the Gibbs-Boltzmann functional for the classical Boltzmann distribution when both steric and correlation effects are not present. Moreover, a new entropy form called the Gibbs-Fermi entropy is proposed here to connect the spatial distribution of ions, water, and voids between them (that may vary) with the change of local probabilities of each species (and void volume) which of course usually have different sizes. The Gibbs-Fermi entropy is a consistent generalization of the global Boltzmann entropy and the classical local Gibbs entropy widely used to describe systems without steric and packing constraints.

The steric effect. The steric effect of crowding produces a steric energy term in PNPF that is a quantitative statement of the crowded charge effect of charge/space competition. The charge/space competition theory introduced by Nonner and Eisenberg to explain calcium selectivity has been developed in a long series of papers using Monte Carlo methods by Boda and Henderson, and density functional methods by Gillespie and collaborators. This ‘all spheres’ approach successfully describes almost all selectivity properties of calcium channels and the main properties of sodium channels such as the micromolar Ca^{2+} affinity for L-type calcium channels [15–17], the wide range of Ca^{2+} affinities for different types of calcium channels, and the switch in selectivity from calcium to sodium when the side chains of the selectivity filter are switched from EEEE (glu glu glu glu) to DEKA (asp glu lys ala) [15, 18]. It also accounts for the selectivity between monovalent cations of different size [19–21] and for the self-organized pore structures for selective ions [22]. In the biologically crucial and special case of Na^+ vs K^+ selectivity in the DEKA sodium channel (so central

to the function of the nervous system and metabolic budget of mammals with large brains [23, 24]), control variables can even be identified that *independently* control selectivity and binding [15, 18].

Interactions. Our main goal is to show how interactions of diffusion, electrophoretic migration, steric exclusion, and imperfect packing of particles can all be treated quantitatively in a unified framework to analyze binding and flow in crowded ion channels, without explicitly calculating forces between individual ions, water, or voids. We show that a Fermi like distribution is able to describe these interactions well enough to account for a wide range of important properties of ions in channels. We wonder how well this approach can describe the myriad of nonideal properties reported in the physical chemistry experimental literature (for more than a century) which have escaped canonical description up to now [25–34].

Numerical results produced by the PNPF model are in accord with the experimental data reported by Almers and McCleskey in 1984 for Ca_v channels over a 10^8 -fold range of concentrations of calcium ions [2]. Their experimental data has been a benchmark for selectivity ever since. Their data has been used as a target for models using a variety of methods ranging from physiological and crystallographic [6], to molecular dynamics (MD) [35, 36], Brownian dynamics (BD) [37–39], Monte Carlo (MC) [15, 17, 40], as well as continuum approaches [41–43].

The remaining part of the paper is organized as follows. A derivation of the configuration entropy of all hard-sphere ions and water with voids is proposed in Section 2, where a Fermi type of excess chemical potential, Gibbs-Fermi free energy functional, and Gibbs-Fermi entropy are also introduced. All these models seem to be new to the literature, as far as we know, because they treat finite size water molecules and voids explicitly. In Section 3, we extend the Gibbs-Fermi theory to the Poisson-Nernst-Planck-Fermi theory for studying ionic transport, steric energy, water density, and void distribution in equilibrium or nonequilibrium conditions. In Section 4, a molecular-continuum model specific to L-type calcium channels is presented to show how to implement in a consistent way the PNPF theory of the molecular filter region of few particles joined to the bath region of numerous particles. Section 5 demonstrates that PNPF currents agree quite well with the experimental currents reported in [2] under the same membrane potential and the same 10^8 -fold range of Ca^{2+} concentrations measured in the experiment. These conductance results seem to fit data better than other models we know of. Some concluding remarks are given in Section 6.

2. FERMI DISTRIBUTION AND GIBBS-FERMI ENTROPY

Based on the configurational entropy model proposed in [12] for aqueous electrolytes with arbitrary K species of nonuniform size, hard spherical ions, we extend the free energy of the model to

$$F(N) = \phi \sum_{j=1}^{K+1} q_j N_j - k_B T \ln W \quad (1)$$

by including specifically the excluded volume effect of the next species ($K + 1$) of water molecules. Here, ϕ is the electrostatic potential, N_j is the total number of j species particles carrying the charge $q_j = z_j e$ with the valence z_j , e is the proton charge, k_B is the Boltzmann constant, and T is the absolute temperature. The volume of a j type particle is $v_j = 4\pi a_j^3/3$ with radius a_j . It is important to note that water is treated as a polarizable hard sphere with zero net charge in Eq. (1), so $z_{K+1} = q_{K+1} = 0$. The polarizability of water and the

inclusion of voids represent important generalizations from the classical primitive solvent model used to describe calcium channels [44]. The last term in (1) describes the mixing entropy of all ions and water molecules over a total of N available nonuniform sites in a system with

$$W = \prod_{j=1}^{K+1} W_j = \frac{N!}{(\prod_{j=1}^{K+1} N_j!) \left(N - \sum_{j=1}^{K+1} N_j\right)!}, \quad (2)$$

where $W_1 = N!/(N_1!(N - N_1)!)$ is the number of combinations for the distribution of N_1 in all vacant sites N . $W_2 = (N - N_1)!/(N_2!(N - N_1 - N_2)!)$ is the number of combinations for the distribution of N_2 in $N - N_1$ vacant sites after N_1 being distributed, and so on. After all particles are distributed, there remains (in this model) just a single site $N_{K+2} = N - \sum_{j=1}^{K+1} N_j = 1$ that is used to represent the (continuously connected) voids created by defects in the packing structure of all particles of all types and by Coulomb and steric forces (e.g., Lennard-Jones) between particles. This void structure is represented as the last species $K + 2$ in our model. We are unaware of other all-spheres models that deal explicitly with the voids between spheres. We suspect that including such voids is needed because voids are in different amounts depending on the composition of the solution and can move in any system of spheres crowded into a small space.

Obviously, all properties of water cannot be represented this way: water is a highly charged molecule although its net charge is zero, and polymeric structures can exist and may be important, along with hydrogen bonds of the low or high energy type [45, 46]. Moreover, not all defects in packing can be represented by a single void site, just as not all properties of water can be represented by uncharged spheres. The question is whether a model that includes only the excluded volume of water and a continuous void space between particles is able to deal with the selectivity data of the calcium channel. We will see that it can.

The total volume V of the system consists of the volumes of all particles and the total void volume v_{K+2} , i.e., $V = \sum_{j=1}^{K+1} v_j N_j + v_{K+2}$. Under the bulk condition, dividing this equation by V yields the bulk void volume fraction

$$\Gamma^B = \frac{v_{K+2}}{V} = 1 - \sum_{j=1}^{K+1} v_j \frac{N_j}{V} = 1 - \sum_{j=1}^{K+1} v_j C_j^B \quad (3)$$

expressed in terms of the nonuniform particle volumes v_j and the bulk concentrations C_j^B of all particle species. We are aware that a model of this sort can be extended into an all-spheres model of ionic solutions of the so called bio-ions Na^+ , K^+ , Ca^{2+} , and Cl^- .

Using the Stirling formula $\ln M! \approx M \ln M - M$ with $M \gg 1$, the electrochemical potential of particle species $i = 1, \dots, K + 1$ is

$$\mu_i = \frac{\partial F(N)}{\partial N_i} = q_i \phi + k_B T \ln \frac{N_i}{N - \sum_{j=1}^{K+1} N_j} \quad (4)$$

from which we deduce global probabilities $P_i = N_i/N$ for all particle species. If we extend our theory by introducing local probabilities $p_i(\mathbf{r}) = v_i C_i(\mathbf{r})$ that depend on location, in effect allowing probabilities to depend on location as in the theory of stochastic processes [47] (applied for example to ionic channels [11, 48, 49]), the electrochemical potential can

be generalized locally to

$$\mu_i(\mathbf{r}) = q_i\phi(\mathbf{r}) + k_B T \ln \frac{v_i C_i(\mathbf{r})}{1 - \sum_{j=1}^{K+1} v_j C_j(\mathbf{r})} = q_i\phi(\mathbf{r}) + k_B T \ln \frac{C_i(\mathbf{r})}{C_i^B} + \mu_i^{\text{ex}}(\mathbf{r}) \quad (5)$$

$$\mu_i^{\text{ex}}(\mathbf{r}) = k_B T \ln \frac{v_i C_i^B}{\Gamma(\mathbf{r})}, \quad \Gamma(\mathbf{r}) = 1 - \sum_{j=1}^{K+1} v_j C_j(\mathbf{r}) = v_{K+2} C_{K+2}(\mathbf{r}), \quad (6)$$

where $C_i(\mathbf{r})$ is the concentration function of spatial variable \mathbf{r} in the solvent domain Ω_s , $\mu_i^{\text{ex}}(\mathbf{r})$ is the excess chemical potential, and $\Gamma(\mathbf{r})$ is the void fraction function with $C_{K+2}(\mathbf{r})$ representing the distribution function of interstitial voids. When $\phi = 0$, $C_i(\mathbf{r}) = C_i^B$ and hence $\mu_i^{\text{ex}} = \mu_i^B = k_B T \ln (v_i C_i^B / \Gamma^B)$ is a constant.

The excess chemical potential is a measure of nonideality that helps understand qualitative behavior. For example, the larger the size v_i of a type i particle, the larger is the activation barrier $\mu_i^{\text{ex}}(\mathbf{r})$ and the harder it is for the particle to make a transition at \mathbf{r} from a local minimum of μ_i^{ex} to another local minimum nearby [50]. The transition mechanism is related to the vacancy configuration as well, i.e., the smaller the value of $\Gamma(\mathbf{r})$, the more crowded the ions are at \mathbf{r} , the harder transition. The excess chemical potential is closely related to the sizes of all particles v_j , their interstitial voids $\Gamma(\mathbf{r})$, their configurations $C_j(\mathbf{r})$, as well as their bulk concentrations C_j^B .

To our knowledge, all existing continuum models do not explicitly take into account the finite size effect of water, let alone the effect of interstitial voids. We did not consider these two effects in our previous work [12] in which water was treated as a single continuous dielectric medium without any voids and the resulting electrochemical potential $\mu_i(\mathbf{r})$ was shown to be a mathematical description of the primitive model of electrolytes, as used in most Monte Carlo and density functional theory models. Our continuum primitive model could well match Monte Carlo (discrete primitive model) results that were obtained in equilibrium state. However, as we proceeded to study nonequilibrium systems using this primitive model, we had difficulty computing the experimental currents reported in [2] due to either inconsistent physics or divergent numerics.

The calcium channel operates very delicately in physiological and experimental conditions as it shifts its exquisitely tuned conductance from Na^+ -flow, to Na^+ -blockage, and to Ca^{2+} -flow when bath Ca^{2+} concentration varies from 10^{-10} to 10^{-2} M. The 10^8 -fold range of experimental conditions make modeling and numerical implementation very challenging. This huge dynamic range was accommodated in our previous work by using an artificial potential to confine mobile oxygen ions of side chains within a filter region, just as that used in all Monte Carlo simulations on the same channel (see e.g. [18]). The artificial potential hindered our effort to match the experimental data since it is a gross approximation of the constraining energy needed to keep the protein atoms in the filter region without specifically considering the void effect. Indeed, using a restraining potential can lead to inconsistencies, since maintaining the steric and electrical potential as conditions change requires injection of energy and charge into the system [51]. We obtain convergent and consistent results using the steric potential in place of the artificial constraining potential of earlier models. The steric potential is an output of our model and varies automatically as conditions change. It has the same units as a confining potential but is as different as the voltages at an input and an output of an ideal amplifier. The following analysis shows that the void species in our model is important not only to describe a consistent physics of the steric potential but also to compute the steric energy that can reflect the 10^8 -fold experimental conditions. It

will be interesting to examine the properties of a model of bulk ionic solutions that contains voids calculated consistently in an all-spheres model of ions and water.

Setting $\mu_i(\mathbf{r}) = \mu_i^{\text{B}}$ (see below for physical reason), the concentration of species i particles can be expressed by the Fermi like distribution function

$$C_i(\mathbf{r}) = C_i^{\text{B}} \exp(-\beta_i \phi(\mathbf{r}) + S^{\text{trc}}(\mathbf{r})), \quad S^{\text{trc}}(\mathbf{r}) = \ln \frac{\Gamma(\mathbf{r})}{\Gamma^{\text{B}}}, \quad (7)$$

where $\beta_i = q_i/k_B T$ and $S^{\text{trc}}(\mathbf{r})$ is called the steric potential that describes the combined effect of all excess chemical potentials μ_j^{ex} of all particle species $j = 1, \dots, K + 1$. The distribution (7) is of Fermi type since all concentration functions

$$C_i(\mathbf{r}) = \frac{\alpha_i - \alpha_i \sum_{j \neq i}^{K+1} v_j C_j(\mathbf{r})}{1 + \alpha_i v_i} < \frac{1}{(1/\alpha_i) + v_i} = \frac{1}{v_i}, \quad (8)$$

$i = 1, \dots, K + 1$, are bounded from above with $\alpha_i = C_i^{\text{B}} \exp(-\beta_i \phi(\mathbf{r})) / \Gamma^{\text{B}} > 0$, i.e., $C_i(\mathbf{r})$ cannot exceed the maximum value $1/v_i$ for any arbitrary (or even infinite) potential $\phi(\mathbf{r})$ at any location \mathbf{r} in the domain Ω_s . In this mean-field Fermi distribution, it is impossible for a volume v_i to be completely filled with particles, i.e., it is impossible to have $v_i C_i(\mathbf{r}) = 1$ (and thus $\Gamma(\mathbf{r}) = 0$) since that would make the excess chemical potential μ_i^{ex} infinitely large or $S^{\text{trc}} = -\infty$ and hence $C_i(\mathbf{r}) = 0$, a contradiction. For this reason, **we must include the voids as a separate species if water is treated as hard spheres**. Otherwise, the volume v_i would be easily filled by particles in the mean-field sense at moderate electric potential such that the steric potential would be unphysical. The requirement of voids when all particles are represented as hard spheres will be justified again from a viewpoint of Gibbs' free energy.

The classical Boltzmann distribution appears if all particles are treated as volumeless points, i.e., $v_i = 0$ and $\Gamma(\mathbf{r}) = \Gamma^{\text{B}} = 1$. It may produce an infinite concentration $C_i(\mathbf{r}) \rightarrow \infty$ in crowded conditions when $-\beta_i \phi(\mathbf{r}) \rightarrow \infty$, close to charged surfaces for example, an impossible result [12–14]. The difficulty in the application of classical Boltzmann distributions to saturating systems has been avoided in the physiological literature (apparently starting with Hodgkin, Huxley, and Katz [52]) by redefining the Boltzmann distribution to deal with systems that can only exist in two states. This redefinition has been vital to physiological research and is used in hundreds of papers [53, 54], but confusion results when the physiologists' saturating two-state Boltzmann is not kept distinct from the unsaturating Boltzmann distribution of statistical mechanics [55].

To further account for the correlation effect of ions and the screening effect of water molecules, we have developed efficient 3D methods [13] for solving the Poisson-Fermi (PF) equation [12–14, 56, 57]

$$\epsilon_s (l_c^2 \nabla^2 - 1) \nabla^2 \phi(\mathbf{r}) = \sum_{i=1}^K q_i C_i(\mathbf{r}) = \rho(\mathbf{r}) \quad (9)$$

self-consistently with Eq. (7) for $\phi(\mathbf{r})$, where l_c is a correlation length [56, 57], $\epsilon_s = \epsilon_w \epsilon_0$, ϵ_w is a dielectric constant of water in the bath, and ϵ_0 is the vacuum permittivity. The fourth-order PF equation reduces to the classical Poisson-Boltzmann (PB) equation when $l_c = S^{\text{trc}}(\mathbf{r}) = 0$. If $l_c \neq 0$, the dielectric operator $\hat{\epsilon} = \epsilon_s (1 - l_c^2 \nabla^2)$ is used to approximate the permittivity of the bulk solvent and the linear response of correlated ions [57]. The dielectric

function $\tilde{\epsilon}(\mathbf{r}) = \epsilon_s/(1 + \eta/\rho)$ is a further approximation of $\hat{\epsilon}$. It is found by transforming Eq. (9) into two second-order equations $\epsilon_s(l_c^2\nabla^2 - 1)\Psi = \rho$ and $\nabla^2\phi = \Psi$. We introduce a density like variable Ψ that yields a polarization charge density $\eta = -\epsilon_s\Psi - \rho$ using Maxwell's first equation [12, 13].

The free energy formula (1) is useful for a thermodynamic system that involves a limited number of particles for MD or MC simulations particularly without flow, or spatially nonuniform boundary conditions. If the system is nonequilibrium or has numerous particles and complicated boundary conditions, the PF equation (9) will be more suitable for theoretical investigation.

Free energy functional. We look at our model now from the perspective of a generalization of free energy that we call the Gibbs-Fermi free energy. The PF equation is a minimizer of the following Gibbs free energy functional

$$G^{\text{Fermi}} = \int_{\Omega_s} d\mathbf{r} \left\{ -\frac{\epsilon_s l_c^2}{2} (\nabla^2 \phi)^2 - \frac{\epsilon_s}{2} |\nabla \phi|^2 + \rho \phi + g \right\} \quad (10)$$

$$g = k_B T \left(\sum_{j=1}^{K+1} \left[C_j \ln(v_j C_j) - C_j - C_j \ln(v_{K+2} C_{K+2}) + \frac{\lambda_j C_j}{k_B T} \right] \right)$$

by taking energy variations with respect to ϕ , i.e., $\frac{\delta G^{\text{Fermi}}}{\delta \phi} = 0$. The Fermi distribution (7) follows from $\frac{\delta G^{\text{Fermi}}}{\delta C_i} = 0$, where

$$\lambda_i = -\mu_i^{\text{B}} = -k_B T \ln \frac{v_i C_i^{\text{B}}}{\Gamma^{\text{B}}} \quad (11)$$

is the Lagrange multiplier for the mass conservation (the total number N_i) of particle species i [58]. The minimization $\frac{\delta G^{\text{Fermi}}}{\delta C_i} = 0$ is equivalent to setting $\mu_i(\mathbf{r}) = \mu_i^{\text{B}}$ for Eq. (7) with the identity $\Gamma = v_{K+2} C_{K+2}$. The electrochemical potential (5) can also be defined by the functional as

$$\mu_i = \frac{\delta G^{\text{Fermi}}}{\delta C_i} + \mu_i^{\text{B}}. \quad (12)$$

When $l_c = S^{\text{trc}}(\mathbf{r}) = v_j = 0$, $j = 1, \dots, K+1$ (without correlation and steric terms), this functional yields the PB equation $-\epsilon_s \nabla^2 \phi(\mathbf{r}) = \rho(\mathbf{r})$ and the Boltzmann distribution $C_i(\mathbf{r}) = C_i^{\text{B}} \exp(-\beta_i \phi(\mathbf{r}))$ since $v_{K+2} C_{K+2} = \Gamma^{\text{B}} = 1$ and $g = k_B T \sum_{j=1}^{K+1} [C_j \ln(C_j/C_j^{\text{B}}) - C_j]$. Note that all v_j in g are canceled before setting $v_j = 0$ since

$$C_j \ln(v_j C_j) + \lambda_j \frac{C_j}{k_B T} = C_j \ln(v_j C_j) - C_j \ln \frac{v_j C_j^{\text{B}}}{\Gamma^{\text{B}}} = C_j \ln \frac{C_j \Gamma^{\text{B}}}{C_j^{\text{B}}}. \quad (13)$$

We need v_j in g to justify that the local electrochemical potential (5) can be defined by the functional (10) and that the Fermi distribution (7) is a consequence of mass conservation by (12).

Voids are needed. To establish a consistent generalization from Boltzmann to Fermi distribution it is critical to express the energy functional (10) by means of the void fraction function $v_{K+2} C_{K+2}(\mathbf{r}) = 1 - \sum_{j=1}^{K+1} v_j C_j(\mathbf{r})$ in g . Otherwise, $\ln(v_{K+2} C_{K+2}(\mathbf{r})) = \ln 1 = 0$ (without the void term) implies that $\sum_{j=1}^{K+1} v_j C_j(\mathbf{r}) = 0$, i.e., all $v_j = 0$ and the Boltzmann functional of volumeless particles that we are seeking to replace. This means that **it is**

impossible to treat all ions and water molecules as hard spheres and at the same time achieve a zero volume of interstitial voids between all particles. Therefore, the Gibbs-Fermi functional (10) is not only consistent but also needed (and of course physical) with either $v_j = 0$ (all particles are volumeless points) or $v_j \neq 0$ (all particles are spheres).

Of course, we could treat ions as spheres but water as a continuous medium (without voids) that then forms the single site in Eq. (2) in place of the voids as previously proposed in our paper [12] for the primitive solvent model. The void fraction $\Gamma(\mathbf{r})$ would then become the water fraction $\Gamma(\mathbf{r}) = 1 - \sum_{j=1}^K v_j C_j(\mathbf{r})$, where the upper limit is K instead of $K+1$. This is precisely the primitive model implemented in the Monte Carlo simulations of Boda and Henderson. Consequently, the primitive model may yield incorrect water densities, pressures, and dielectric coefficient in mean-field sense for nonideal and inhomogeneous systems (see Section 5 for more details). This important limitation in the continuous water version of the all-spheres model was pointed out early in its history [44].

Comparison with other treatments of finite sized particles. All existing free energy functionals that specifically include either uniform size ($v = v_j$ for all j) [57, 59–62] or nonuniform sizes ($v_i \neq v_j$) [13, 63, 64] cannot reduce to their corresponding Boltzmann functionals by directly setting $v_j = 0$ [60, 64] because those functionals retain the local probability form of $v_j C_j \ln(v_j C_j) = p_j \ln p_j$ in their Gibbs entropy. They use an inconsistent reciprocal term involving a *uniform* particle size, namely $1/v$, instead of a consistent term involving the nonuniform particle sizes. The local probability $p_j(\mathbf{r})$ of any particle species j in our Gibbs entropy

$$-k_B \sum_{j=1}^{K+1} C_j \ln(v_j C_j) - C_j \ln(v_{K+2} C_{K+2}) + \frac{\lambda_j C_j}{k_B T} = -k_B \sum_{j=1}^{K+1} C_j \ln \frac{C_j \Gamma^B}{C_j^B \Gamma} \quad (14)$$

is instead expressed in terms of the local probability ratio $C_j(\mathbf{r})/\Gamma(\mathbf{r})$ and the global probability ratio Γ^B/C_j^B between the particle fraction (probability) $C_j(\mathbf{r})$ and the void fraction $\Gamma(\mathbf{r})$ per unit volume. In other words, the local probability $p_j(\mathbf{r})$ in the Gibbs-Fermi treatment changes with varying configurations of all particles ($\Gamma(\mathbf{r}) = 1 - \sum_{j=1}^{K+1} v_j C_j(\mathbf{r})$) and voids ($\Gamma(\mathbf{r}) = v_{K+2} C_{K+2}(\mathbf{r})$). The local probability at any location, including the binding site, is also connected to the bulk conditions in the bath as implied by Eq. (7). It also depends implicitly on the sizes of all particles, valences of ionic species, and long range (Coulomb) as well as short range (Lennard-Jones) distances between all particles. All these physical properties are lumped into the steric potential functional $S^{\text{trc}}(\mathbf{r}) = \ln \frac{\Gamma(\mathbf{r})}{\Gamma^B}$ in a very simple and unified way.

The void fractions Γ^B and Γ represent the Lennard-Jones distances between all particles in a mean-field approximation. More specifically, the L-J potential $V(r) = 4((\sigma/r)^{12} - (\sigma/r)^6)$ [65] can be used to determine the distance r between any pair of particles. In bulk solutions, the distance $r = \sigma$ yields $V(r) = 0$ that corresponds to a finite but fixed distance σ between any two adjacent particles in the system and thus to the constant bulk void fraction Γ^B . Similarly, the nonuniform void function $\Gamma(\mathbf{r})$ corresponds to nonuniform inter-particle distances r that may or may not equal σ for all pairs of adjacent particles. Nonzero L-J potentials are in general highly oscillatory and extremely expensive to compute in a system of numerous particles. Including external fields adds problems of consistency with spatially nonuniform far field boundary conditions to the problems of computational expense. The void function $\Gamma(\mathbf{r})$ or equivalently the steric potential $S^{\text{trc}}(\mathbf{r})$ is on the other hand quite smooth and relatively very easy to compute. The convolutional density functional on any

pair of concentration functions $C_i(\mathbf{r})$ and $C_j(\mathbf{r}')$ with a L-J kernel or DFT representation of the interaction potential proposed by Eisenberg et al. [66] is another mean-field approximation, which is more accurate (but much more difficult to compute reliably) than the steric potential $S^{\text{trc}}(\mathbf{r})$ since the convolutional functional is nonlocal whereas $S^{\text{trc}}(\mathbf{r})$ is local. The local steric potential of this paper can be used in place of the nonlocal L-J or DFT potential of [66] and therefore the energy variational theory based on the Onsager dissipation principle developed in [66] can be applied to the Gibbs-Fermi functional (10).

3. POISSON-NERNST-PLANCK-FERMI THEORY

For nonequilibrium systems, the classical PNP model [9–11] can then be generalized to the Poisson-Nernst-Planck-Fermi model by coupling the flux density equation

$$\frac{\partial C_i(\mathbf{r}, t)}{\partial t} = -\nabla \cdot \mathbf{J}_i(\mathbf{r}, t), \quad \mathbf{r} \in \Omega_s \quad (15)$$

of each particle species $i = 1, \dots, K + 1$ (including water) to the PF equation (9), where the flux density is defined as

$$\mathbf{J}_i(\mathbf{r}, t) = -D_i [\nabla C_i(\mathbf{r}, t) + \beta_i C_i(\mathbf{r}, t) \nabla \phi(\mathbf{r}, t) - C_i(\mathbf{r}, t) \nabla S^{\text{trc}}(\mathbf{r}, t)], \quad (16)$$

D_i is the diffusion coefficient, and the time variable t is added to describe the dynamics of electric $\phi(\mathbf{r}, t)$ and steric $S^{\text{trc}}(\mathbf{r}, t)$ potentials. The flux equation (15) is called the Nernst-Planck-Fermi equation because the Fermi steric potential $S^{\text{trc}}(\mathbf{r}, t)$ is introduced to the classical NP equation.

At equilibrium, the net flow of each particle species is a zero vector, i.e., $\mathbf{J}_i(\mathbf{r}) = \mathbf{0}$ (in a steady state) which implies that $C_i \exp(\beta_i \phi - S^{\text{trc}}) = \text{const.} = C_i^{\text{B}}$ for $\phi = S^{\text{trc}} = 0$. Therefore, the NPF equation (15) reduces to the Fermi distribution (7) at equilibrium. Similarly, the classical NP equation reduces to the Boltzmann distribution at equilibrium.

The steric force. The gradient of the steric potential ∇S^{trc} in (16) represents an entropic force of vacancies exerted on particles. The negative sign in $-C_i \nabla S^{\text{trc}}$ means that the steric force ∇S^{trc} is in the opposite direction to the ‘diffusional’ force ∇C_i .

The larger $S^{\text{trc}}(\mathbf{r}) = \ln \frac{\Gamma(\mathbf{r})}{\Gamma^{\text{B}}}$ (meaning more space available to the particle as implied by the numerator) at \mathbf{r} in comparison with that of neighboring locations, the more the entropic force pushes the particle to the location \mathbf{r} , which is simply the opposite mechanism of the diffusional force $\nabla C_i(\mathbf{r})$ that pushes the particle away from \mathbf{r} if the concentration is larger at \mathbf{r} than that of neighboring locations. Moreover, the Nernst-Einstein relationship [8] implies that the steric flux $D_i C_i \nabla S^{\text{trc}}$ is greater if the particle is more mobile. Therefore, the gradients of electric and steric potentials ($\nabla \phi$ and ∇S^{trc}) describe the charge/space competition mechanism of particles in a crowded region within a mean-field framework. Since $S^{\text{trc}}(\mathbf{r}, t)$ describes the dynamics of void movements, the dynamic crowdedness (pressure) of the flow system can also be quantified.

The motion of water molecules is directly controlled by the steric potential in our model and their distributions are expressed by $C_{K+1}(\mathbf{r}, t) = C_{K+1}^{\text{B}} \exp(S^{\text{trc}}(\mathbf{r}, t))$. Nevertheless, this motion is still implicitly affected by the electric potential $\phi(\mathbf{r}, t)$ via the correlated motion of ions described by other $C_j(\mathbf{r}, t)$ in the void fraction function $\Gamma(\mathbf{r}, t)$ and hence in the charge density ρ in (9).

Water is polarizable in our model. From (9), $\nabla^2\phi = \Psi$, and $\eta = -\epsilon_s\Psi - \rho$, we deduce that the Poisson equation

$$-\epsilon_s\nabla^2\phi = \rho - \epsilon_sl_c^2\nabla^2\Psi = \rho + \eta, \quad (17)$$

which describes the electric field $\mathbf{E} = -\nabla\phi$ in the system, contains the charge source not only from the ions ($\rho = \sum_{i=1}^K q_i C_i$) but also from the polar water (η) provided that the correlation length $l_c \approx l_B q_i^2$ is not zero. The polarization charge density η is proportional to the fourth order of the ionic valence z_i . The fourth order dependence shows that even in a mean field theory valency of ions is expected to play an important role as known in chemical and biological systems [5, 12–14, 17, 57, 67].

In summary, the PNPF model accounts for the steric effect of ions and water molecules, the correlation effect of crowded ions, the screening effect of polar water, as well as the charge/space competition effect of ions and water molecules of different sizes and valences. These effects are all closely related to the interstitial voids between particles and described by two additional terms, namely, the correlation length and the steric potential.

4. A MOLECULAR-CONTINUUM MODEL OF A CALCIUM CHANNEL

To test the PNPF theory, we use the Lipkind-Fozzard molecular model [35] of L-type Ca channels in which the EEEE locus (four glutamate side chains modeled by 8 $O^{1/2-}$ ions) forms a high-affinity Ca^{2+} binding site that is essential to Ca^{2+} selectivity, blockage, and permeation. We refer to Fig. 9 in [35] or Fig. 1 in [14] for a 3D illustration of the EEEE locus. A 2D cross section of a simplified 3D channel geometry for the present work is shown in Fig. 1, where the central circle denotes the binding site, the other four circles denote the side view of 8 $O^{1/2-}$ ions, Ω_s is the solvent region consisting of two baths and the channel pore including the binding domain $\overline{\Omega}_{\text{Bind}}$, $\partial\Omega_s$ is the solvent boundary, and $\partial\Omega_{\text{Bath}}$ is the outside and inside bath boundary. Fig. 2 is a sketch of the binding site and $O^{1/2-}$ ions, where d_O^{Ca} is the distance between the center of a binding Ca^{2+} ion and the center c_j of any $O^{1/2-}$, and A is any point on the surface of the site. In our model, the 8 $O^{1/2-}$ ions are not contained in the solvent region Ω_s . Particle species are indexed by 1, 2, 3, and 4 for Na^+ , Ca^{2+} , Cl^- , and H_2O with radii $a_1 = a_{Na^+} = 0.95$, $a_2 = a_{Ca^{2+}} = 0.99$, $a_3 = r_{Cl^-} = 1.81$, and $a_4 = a_{H_2O} = 1.4 \text{ \AA}$, respectively.

In [14], we proposed an algebraic model for calculating the electrical potential $\overline{\phi}_b$ and the steric potential $\overline{S}_b^{\text{trc}}$ in $\overline{\Omega}_{\text{Bind}}$ by using Coulomb's law with the atomic structure of binding ion and atoms in a channel protein as shown in Fig. 2, without solving the Poisson-Fermi equation (9) in $\overline{\Omega}_{\text{Bind}}$. The binding potential $\overline{\phi}_b$ is then used as a Dirichlet boundary condition in $\overline{\Omega}_{\text{Bind}}$ for solving the PF equation in the solvent region between the bath and binding boundary, i.e., in $\Omega_s \setminus \overline{\Omega}_{\text{Bind}}$, to obtain the potential profile $\phi(\mathbf{r})$ that connects $\overline{\phi}_b$ in $\overline{\Omega}_{\text{Bind}}$ to the potential V_i (or V_o) on the inside (or outside) bath boundary.

The filter domain defined in [14] is simply taken to be the binding domain $\overline{\Omega}_{\text{Bind}}$ in this paper. The volume of this domain is an unknown variable v_b that changes with different charges in the binding site. We do not define an ad hoc filter for which its volume is fixed to one value in one implementation and possibly to another value in other implementation. We show that the variable binding volume v_b plays an essential role in determining the steric potential in and around the binding site and consequently the hydrophobicity of the EEEE locus under different bath conditions.

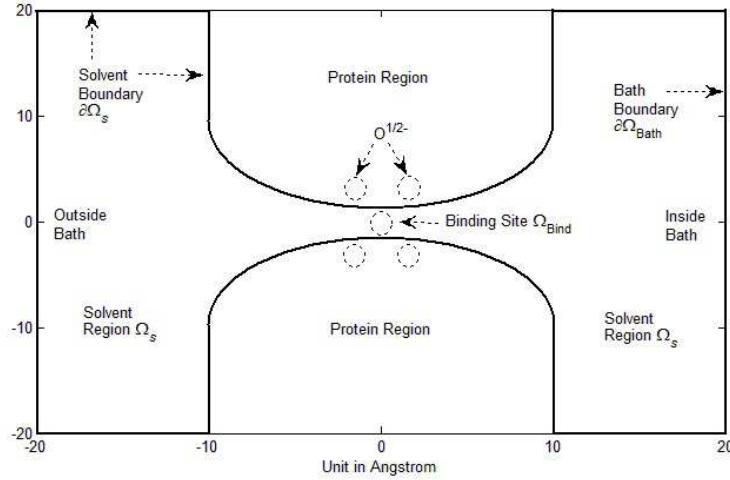


FIG. 1: A simplified Ca channel geometry with baths, pore, and binding site. The channel is placed in a cubic box with the length of each side being 40 Å. The solvent region Ω_s consists of two baths and the channel pore with the boundary $\partial\Omega_s$. The binding site $\bar{\Omega}_{\text{Bind}}$ is contained in Ω_s but the $O^{1/2-}$ ions are not in Ω_s . The outside and inside bath boundary is denoted by $\partial\Omega_{\text{Bath}}$.

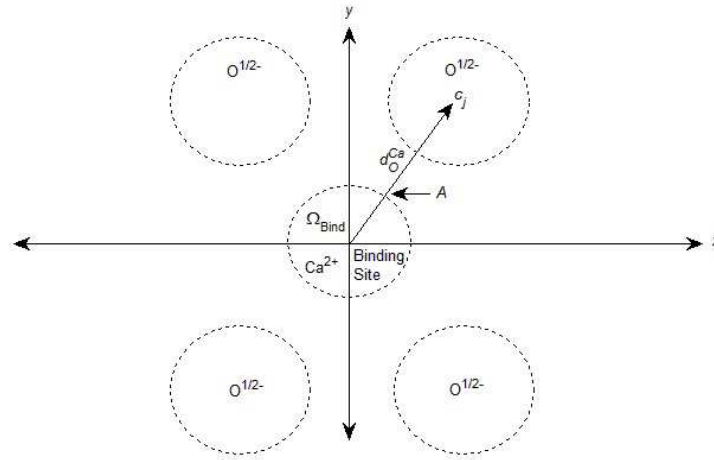


FIG. 2: The binding distance between the center of the binding Ca^{2+} ion and the center c_j of the j^{th} $O^{1/2-}$ ion is denoted by d_O^{Ca} for $j = 1, \dots, 8$. A is any point on the surface of the binding ion.

The algebraic model [14] is defined in $\bar{\Omega}_{\text{Bind}}$ and consists of the following equations

$$\begin{cases} O_1^b = v_b C_1^{\text{B}} \exp(-\beta_1 \bar{\phi}_b + \bar{S}_b^{\text{trc}}) \\ O_2^b = v_b C_2^{\text{B}} \exp(-\beta_2 \bar{\phi}_b + \bar{S}_b^{\text{trc}}) \\ O_4^b = v_b C_4^{\text{B}} \exp(\bar{S}_b^{\text{trc}}) \end{cases}, \quad (18)$$

$$\bar{S}_b^{\text{trc}} = \ln \frac{v_b - v_1 O_1^b - v_2 O_2^b - v_4 O_4^b}{v_b \Gamma^{\text{B}}} \quad (19)$$

$$\frac{e}{4\pi\epsilon_0} \left(\sum_{j=1}^8 \frac{z_{O^{1/2-}}}{|c_j - A|} + \frac{O_1^b z_{Na^+}}{a_{Na^+}} + \frac{O_2^b z_{Ca^{2+}}}{a_{Ca^{2+}}} \right) = \bar{\phi}_b, \quad (20)$$

where O_1^b , O_2^b , and O_4^b denote the occupancy numbers of Na^+ , Ca^{2+} , and H_2O in v_b , respectively, $\bar{\phi}_b$ and \bar{S}_b^{trc} are average electrical and steric potentials, and $|c_j - A|$ is the distance between A and c_j in Fig. 2.

In this mean field, we allow O_1^b and O_2^b (and hence the total charge $O_1^b e z_{Na^+} + O_2^b e z_{Ca^{2+}}$) to vary continuously subject to the condition on their sum $O_1^b + O_2^b = 1$ in the binding volume v_b . Eqs. (18) and (19) uniquely determine the four unknowns v_b , O_4^b , $\bar{\phi}_b$ and \bar{S}_b^{trc} with O_1^b and O_2^b being given. Eq. (20) uniquely determines the locations (c_j) of 8 $O^{1/2-}$ ions (and thus the binding distance d_O^{Ca} or d_O^{Na} in Fig. 2) once $\bar{\phi}_b$ is obtained. Note that the binding distance $d_O^{O_1^b Na + O_2^b Ca}$ (or c_j) changes continuously with varying O_1^b and O_2^b but $\bar{\phi}_b$ remains fixed, where the binding ion $O_1^b Na + O_2^b Ca$ is a linear combination of Na^+ and Ca^{2+} . Therefore, $O^{1/2-}$ ions are movable — the protein is flexible in our model — as their locations c_j changes with varying O_1^b and O_2^b [14]. Note that we change the probability notation P_i in [14] to the occupancy notation O_i^b to reflect the deterministic, instead of probabilistic, nature of the PNPF continuum model. In this simple algebraic model, we do not consider the hydrogen ions that may react with carboxyl anions in the protein. Experiments done at pH 8 (as many have been done) do not involve association of hydrogen ions with carboxyl anions.

For the half-blockage experimental condition [2]

$$\underbrace{C_{Na^+}^B = C_1^B = 32 \text{ mM}, C_{Ca^{2+}}^B = C_2^B = 0.9 \text{ }\mu\text{M}}_{\text{Experimental Data}}, \quad (21)$$

we follow convention and assume relative occupancies of a filled channel, $O_1^b = 0.5$ and $O_2^b = 0.5$, and thereby obtain $\bar{\phi}_b = -10.48 k_B T/e$, $\bar{S}_b^{\text{trc}} = -1.83$, and $v_b = 4.56 \text{ \AA}^3$ [14]. The binding experiments [2] used a fixed $C_{Na^+}^B = C_1^B = 32 \text{ mM}$ and various Ca^{2+} bath concentrations $C_{Ca^{2+}}^B = C_2^B$ that imply different O_1^b and O_2^b of Na^+ and Ca^{2+} occupying the binding site. The occupancy numbers O_1^b and O_2^b are determined by

$$\frac{O_1^b}{O_2^b} = \frac{1 - O_2^b}{O_2^b} = \exp(-(\beta_1 - \beta_2)\bar{\phi}_b) \frac{C_1^B}{C_2^B}, \quad (22)$$

where $\bar{\phi}_b$ was just obtained from the case of equal occupancy. The occupancy ratio in (22) thus deviates from unity as C_2^B is varied along the horizontal axis of the binding curve from its midpoint value $C_2^B = 0.9 \text{ }\mu\text{M}$ as shown in Fig. 5 in [14].

Keeping $\bar{\phi}_b$ fixed is equivalent to assuming that the relation (22) between the occupancy and bath concentration ratios is linear [14]. Moreover, keeping $\bar{\phi}_b$ fixed in (20) is equivalent to assuming that the $O^{1/2-}$ ions (c_j) move continuously in response to the continuous change of charges $O_1^b z_{Na^+} + O_2^b z_{Ca^{2+}}$ in the binding site. In [14], the charge change from z_{Na^+} (Na^+ occupying the site) to $z_{Ca^{2+}}$ (Ca^{2+} occupying the site) reflects a change of pore radius of about 2.3 \AA that is surprisingly close to the value of 2 \AA obtained by MD simulations [36]. Note that the vacuum permittivity ϵ_0 is chosen in (20) since both MD models in [35, 36] treat $O^{1/2-}$ ions explicitly as shown in Fig. 1 (or Fig. 9 in [35]). The Coulomb forces between the binding ion and $O^{1/2-}$ ions should therefore be calculated in vacuum since nothing is

in between these ions. Our numerical results can thus be verified with those of MD. Of course, our assumptions in the linear model should be modified if more accurate structural information can be used to provide an extra equation for variable $\bar{\phi}_b$. The permittivity is chosen as $30\epsilon_0$ [14] in our forthcoming studies on the protein structure of a sodium/calcium exchanger (NCX) [68]. Meanwhile, the linear model seems at least as good as the homology structure itself, and provides potentially useful and interesting insights as we show in the results section. Nevertheless, we imagine that nature might design flexible proteins so that $\bar{\phi}_b$ is fixed or slightly perturbed by small thermal variations so that the linear model is still tolerable within numerical errors in theoretical simulations.

The simple atomic structure in Fig. 2 elucidates algebraic and subsequent PNP calculations in a concise way. The molecular-continuum model presented here can be extended to deal with more complex nonequilibrium systems in real protein channels in future studies. Application of the algebraic model to the NCX structure [68] is briefly discussed in [14]. It will be interesting to apply the present model to recent structures of a TRPV1 ion channel [69] and a voltage gated calcium channel [6].

For nonequilibrium cases, the binding steric potential \bar{S}_b^{trc} is assigned its equilibrium value in subsequent PNP calculations, i.e., the void fraction $\Gamma(\mathbf{r})$ in $\bar{\Omega}_{\text{Bind}}$ is assumed to remain unchanged from equilibrium to nonequilibrium. The electrical potential $\bar{\phi}_b$ will be modified by the membrane potential $V_i - V_o$ [70] and then used as a Dirichlet type condition for the potential function $\phi(\mathbf{r})$ in $\bar{\Omega}_{\text{Bind}}$. We summarize the boundary conditions for the PF (9) and NPF (15) equations defined in the solvent region Ω_s in Fig. 1 as

$$\left\{ \begin{array}{l} \phi(\mathbf{r}) = \tilde{\phi}_b(\mathbf{r}) \text{ in } \bar{\Omega}_{\text{Bind}}, \phi(\mathbf{r}) = V_{o,i} \text{ on } \partial\Omega_{\text{Bath}}, \\ \nabla\phi(\mathbf{r}) \cdot \mathbf{n} = 0 \text{ on } \partial\Omega_s \setminus \partial\Omega_f, \\ C_1(\mathbf{r}) = C_1^{\text{B}} = [\text{Na}^+]_{o,i}, C_2(\mathbf{r}) = C_2^{\text{B}} = [\text{Ca}^{2+}]_{o,i}, C_3(\mathbf{r}) = C_3^{\text{B}} = [\text{Cl}^-]_{o,i} \text{ on } \partial\Omega_{\text{Bath}}, \\ \mathbf{J}_i(\mathbf{r}) \cdot \mathbf{n} = 0 \text{ on } \partial\Omega_s \setminus \partial\Omega_{\text{Bath}}, \end{array} \right. \quad (23)$$

where \mathbf{n} is an outward unit vector on the solvent boundary $\partial\Omega_s$. Note that the electrostatic potential $\phi(\mathbf{r})$ is prescribed as a Dirichlet function $\tilde{\phi}_b(\mathbf{r})$ whose spatial average in $\bar{\Omega}_{\text{Bind}}$ is the constant $\bar{\phi}_b$. However, the binding domain $\bar{\Omega}_{\text{Bind}}$ is treated as an interior domain instead of boundary domain for the flux equation (15). An iterative process of solving PF (9) and then NPF (15) is repeated until self-consistent solutions of $\phi(\mathbf{r})$ and $C_i(\mathbf{r})$ are reached within a tolerable error bound.

Treating the interior domain $\bar{\Omega}_{\text{Bind}} \subset \Omega_s$ in place of the conventional boundary $\partial\Omega_s$ for the potential condition $\phi(\mathbf{r}) = \tilde{\phi}_b(\mathbf{r})$ is not a conventional way to solve the Poisson equation. This method is needed because the binding potential $\bar{\phi}_b$ determined by (18)-(20) is coupled to the steric potential \bar{S}_b^{trc} that in turn depends crucially on the conformation of the binding ion and protein atoms, their interstitial voids, and their charges as shown in Fig. 2. Water also plays a vital role as in (19). The steric equation (19) is in the interior domain $\bar{\Omega}_{\text{Bind}}$. In other words, for calculating \bar{S}_b^{trc} we need to consider voids and water volume that are interior quantities in $\bar{\Omega}_{\text{Bind}}$ and cannot be specified on the solvent boundary $\partial\Omega_s$. We thus need to impose $\phi(\mathbf{r}) = \tilde{\phi}_b(\mathbf{r})$ in $\bar{\Omega}_{\text{Bind}}$ because $\tilde{\phi}_b(\mathbf{r})$ is given by $\bar{\phi}_b$ in $\bar{\Omega}_{\text{Bind}}$.

If a conventional method is used to solve the Poisson (or PF) equation [13], the resulting steric potential \bar{S}_b^{trc} (as an output of $\phi(\mathbf{r})$ by (7)) may be completely incorrect in $\bar{\Omega}_{\text{Bind}}$ because the atomic equations (19) and (20) are not used. We do not have any differential equation for the steric function $S^{\text{trc}}(\mathbf{r})$ for which appropriate boundary conditions near $\bar{\Omega}_{\text{Bind}}$ can be imposed if a conventional method is used. Moreover, the important role of water and

its volume effect is not taken into account in conventional methods or models.

The models and methods proposed in this paper are still coarse approximations to ion transport as the PNPF theory is in its early development. Nevertheless, the theory proposed here provides many atomic properties such as (19) and (20) that have been shown to be important for studying the binding mechanism in Ca_V channels [14] and are also important for the transport mechanism as shown in the next section. Incorporating atomic properties into continuum models is a step forward to improve and refine the continuum theory that has been challenged for its accuracy when compared to (mostly equilibrium calculations) MC, BD, or MD [5, 37, 71, 72]. Continuum models on the other hand have substantial advantages in efficiency that are of great importance in studying a range of conditions and concentrations, as are present in experiments.

5. RESULTS

Ca_V channel conducts primarily Na^+ when the Ca^{2+} concentration is below $1 \mu\text{M}$ but it conducts primarily Ca^{2+} in the physiological concentration range mM. In [2], 19 extracellular solutions and 3 intracellular solutions were studied experimentally. The range of $[\text{Ca}^{2+}]_o$ is 10^8 -fold from $10^{-10.3}$ to 10^{-2} M as given in [2]. Explaining the biological function of trace Ca^{2+} concentrations is a crucial task of biophysical models while dealing with the large Ca^{2+} concentrations found in extracellular solutions of all biological systems. This range of calcium concentrations poses severe obstacles for MD and BD simulations even on the most advanced computers to date [73]. To our knowledge, a comparison of MD simulations with experimental measurements [2] has not yet been reported without invoking arbitrary (i.e., untested) extrapolation methods for handling the 10^8 -fold variation of concentration and the dynamics of ionic flow [73, 74].

PNPF results are in accord with the experimental data in [2] as shown in Fig. 3 under only the same salt conditions of NaCl and CaCl_2 in pure water, without considering protons and other bulk salts in experimental solutions. With $[\text{Na}^+]_i = [\text{Na}^+]_o = 32 \text{ mM}$ and $[\text{Ca}^{2+}]_i = 0$, the membrane potential is fixed at -20 mV ($V_o = 0$ and $V_i = -20 \text{ mV}$) throughout, as assumed in Fig. 11 of [2] for all single-channel currents (in femto ampere fA) recorded in the experiment. Note that the experimental currents have been converted to single-channel currents in Fig. 11 of [2] as shown on the right hand y -axis in that figure. The currents are on the femtoscale because calcium channels have been long recognized to be in some sense blocked sodium channels and here too we have small membrane potentials. The small circles in Fig. 3 denote the estimated currents (by eye) from Fig. 11 of [2] and the plus sign denotes the current calculated by PNPF. The channel is almost blocked by Ca^{2+} ions with a current of about 15 fA at $[\text{Ca}^{2+}]_o = 10^{-4.2} \text{ M}$. Half-blockage current (about 77 fA) is defined by the one half of the saturation current (about 154 fA at $[\text{Ca}^{2+}]_o = 10^{-10.3} \text{ M}$). The half-blockage Ca^{2+} concentration is about $[\text{Ca}^{2+}]_o = 0.9 \mu\text{M}$ and that is used to define the midpoint binding condition (21).

PNPF deals naturally with the main experimental data of ionic flow based on this binding definition. Physical parameters in (9) and (16) are summarized in Table 1 with their physical meaning, numerical values, and units for ease of reference. The diffusion coefficient in the channel pore is taken as $\theta_i D_i$ for each ionic species, where D_i are bulk values in the table and $\theta_i = 0.1$ are factors for the pore. All physical parameters are kept fixed throughout.

PNPF can provide more physical details of ion transport inside the channel pore such as electrical potential ($\phi(\mathbf{r})$ in Fig. 4), steric potential ($S^{\text{trc}}(\mathbf{r})$ in Fig. 5), energy wells ($\mathcal{E}_2(\mathbf{r})$

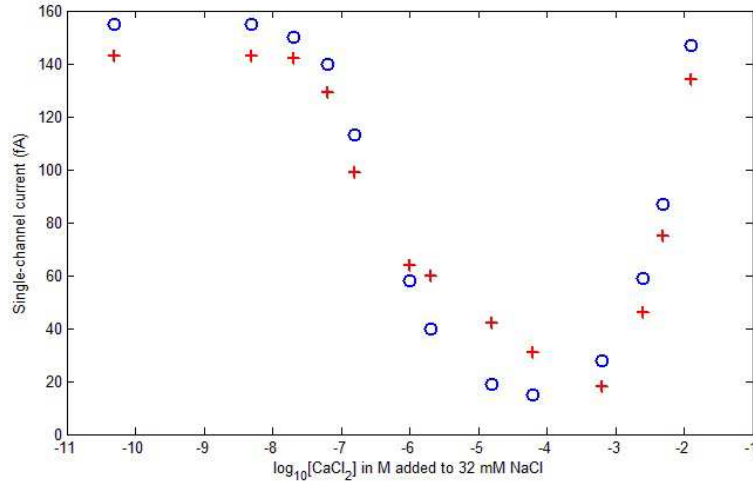


FIG. 3: Anomalous Mole Fraction Effect. Single-channel inward current in femto ampere (fA) plotted as a function of $\log_{10}[\text{Ca}^{2+}]_o$. Experimental data marked by small circles are those in [2] whereas the PNPf data are denoted by the plus sign.

in Fig. 6), water density ($C_4(\mathbf{r})$ shown in Fig. 7), void volume fraction ($\Gamma(\mathbf{r})$ in Fig. 8), dielectric function ($\tilde{\epsilon}(\mathbf{r})$ in Fig. 9), crowded ions in binding site (Fig. 10), concentrations ($C_2(\mathbf{r})$ in Fig. 11), and flux densities ($|\mathbf{J}_2(\mathbf{r})|$ in Fig. 12). The electric potential profiles remain almost unchanged for various C_2^B as shown in Fig. 4 following the linear model of the occupancy equation (22).

What is new? The steric potential profiles shown in Fig. 5 represent the novelty of the PNPf theory. All effects of volume exclusion, interstitial void, configuration entropy, short range interactions, correlation, polarization, screening, and dielectric response of this nonideal system are described by the steric functional $S^{\text{trc}}(\mathbf{r})$. The Ca^{2+} energy landscape $\mathcal{E}_2(\mathbf{r}) = (\beta_2\phi(\mathbf{r}) - S^{\text{trc}}(\mathbf{r}))k_B T$ (Fig. 6) is modified by this potential. The steric potential in the binding region decreases drastically from -1.30 to $-10.34 k_B T$ as C_2^B increases from $10^{-7.2}$ to 10^{-2} M. The water density $C_4(\mathbf{r}) = C_4^B \exp(S^{\text{trc}}(\mathbf{r}))$ (Fig. 7) and the void volume $\Gamma(\mathbf{r})$ (Fig. 8) decrease as well because more Ca^{2+} ions in the bath make the binding site more crowded as was previously seen in the algebraic Fermi model [14].

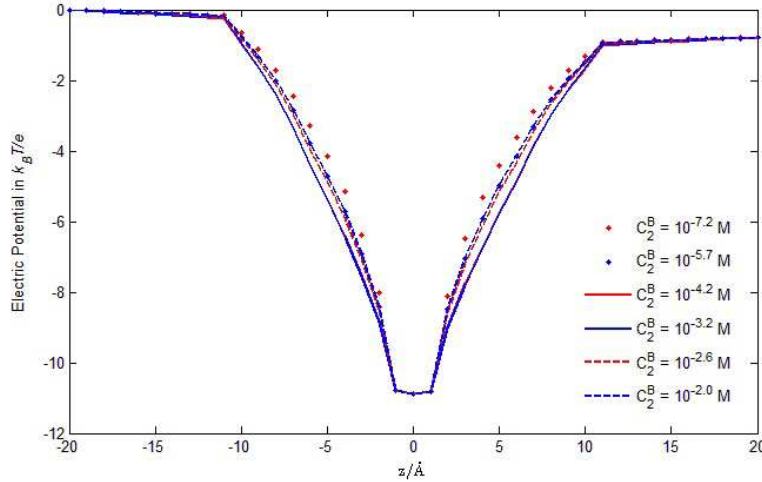


FIG. 4: The electrical potential $\phi(\mathbf{r})$ profiles (averaged over each cross section) along the pore axis for various C_2^B ranging from $10^{-7.2}$ M to 10^{-2} M. All the following figures are obtained with the same averaging method and the same range of C_2^B .

Table 1. Notations and Physical Constants

Symbol	Meaning	Value	Unit
k_B	Boltzmann constant	1.38×10^{-23}	J/K
T	temperature	298.15	K
e	proton charge	1.602×10^{-19}	C
ϵ_0	permittivity of vacuum	8.85×10^{-14}	F/cm
ϵ_w	water dielectric constant	78.5	
l_c	correlation length	1.98	Å
D_1	Na ⁺ diffusion coefficient	1.334×10^{-5}	cm ² /s
D_2	Ca ²⁺ diffusion coefficient	0.792×10^{-5}	cm ² /s
D_3	Cl ⁻ diffusion coefficient	2.032×10^{-5}	cm ² /s
C_1^B	Na ⁺ bath concentration	32	mM
C_2^B	Ca ²⁺ bath concentration	$10^{-10.3} \sim 10^{-2}$	M
$V_{i,o}$	inside (outside) voltage	0 (-20)	mV

In physiological bath conditions $C_2^B = 10^{-2} \sim 10^{-3}$ M, Fig. 7 shows that the region containing the binding site with the length about 10 \AA is very dry (hydrophobic), which agrees with the recent crystallographic analysis [68] of the Ca²⁺ binding site of the related protein NCX with the EETT locus showing a hydrophobic patch (also about 10 \AA in length) formed by the conserved Pro residues. The hydrophobicity near the binding site in our model is described by the continuous water density function $C_4(\mathbf{r})$ via the continuous steric function $S^{\text{trc}}(\mathbf{r})$ as shown in Fig. 5. At $C_2^B = 10^{-2}$ M, the magnitude of the steric energy $S^{\text{trc}} = -10.34 k_B T$ is comparable to that of the electrostatic energy $\phi = -10.48 k_B T/e$. This surprisingly large energy due only to the steric effect has not been quantified and observed by MD, MC, or other continuum methods in Ca_v channel modeling, as far as we know. As observed from Fig. 3, ionic transport is blocked by the competition between Na⁺ and Ca²⁺

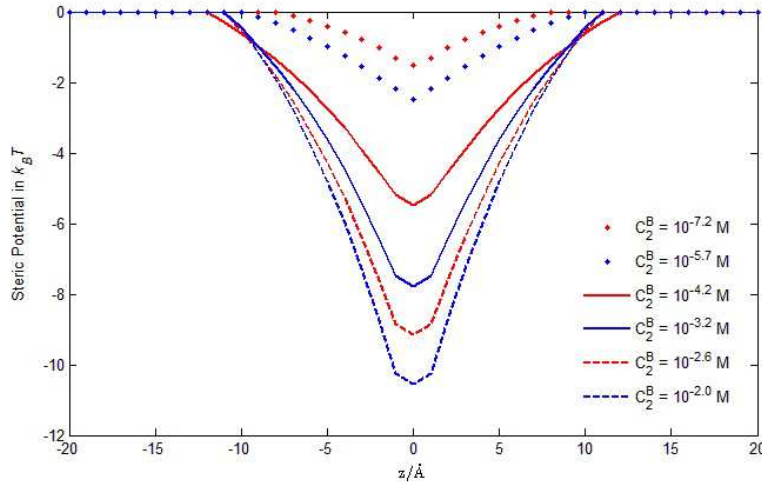


FIG. 5: The averaged steric potential $S^{\text{trc}}(\mathbf{r})$ profiles.

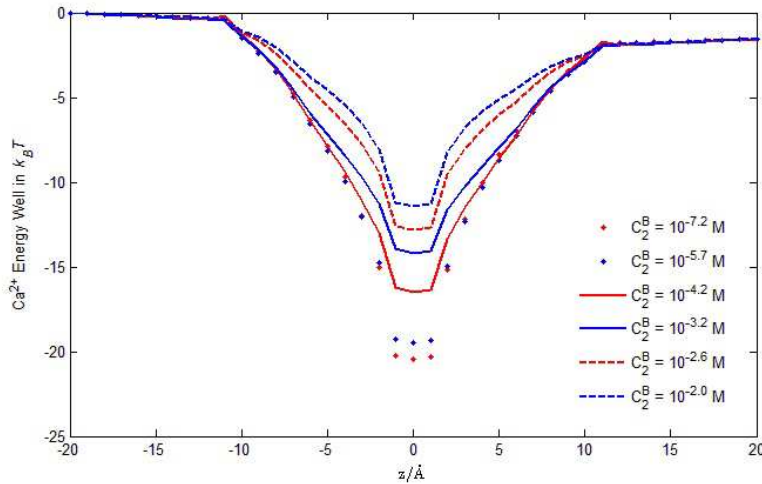


FIG. 6: The averaged Ca^{2+} energy well $\mathcal{E}_2(\mathbf{r})$ profiles.

ions in the range $C_2^{\text{B}} = 10^{-5.7} \sim 10^{-4.2}$ M. In this blocking range, the corresponding steric profiles in Fig. 5 are wider indicating that the water density or the void volume is more evenly distributed.

Fig. 9 demonstrates the combined effects of correlation, polarization, and screening in this highly inhomogeneous electrolyte by means of the variation of dielectric coefficient produced by the Poisson-Fermi equation (9). Note that the dielectric function can also be calculated by $\tilde{\epsilon}(\mathbf{r}) = \epsilon_b + C_4(\mathbf{r})(\epsilon_w - \epsilon_b)/C_4^{\text{B}}$ using the water density function $C_4(\mathbf{r})$ as proposed in [75], where $\epsilon_b = 2$. Fig. 10 illustrates how ions crowd in the highly charged binding site and, in the meantime, voids and water vacate under the condition $C_2^{\text{B}} = 10^{-5.7}$ M.

The Ca^{2+} occupancy O_2^{b} in the binding site increases from 0.69 (not shown) at $C_2^{\text{B}} = 10^{-5.7}$ M to almost 1 at $C_2^{\text{B}} = 10^{-2}$ M. The corresponding peak Ca^{2+} concentration shown in Fig.

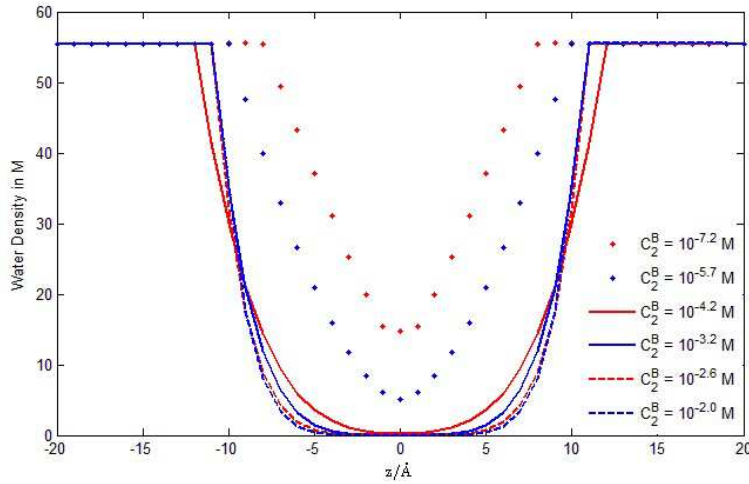


FIG. 7: The averaged water density $C_4(\mathbf{r})$ profiles.

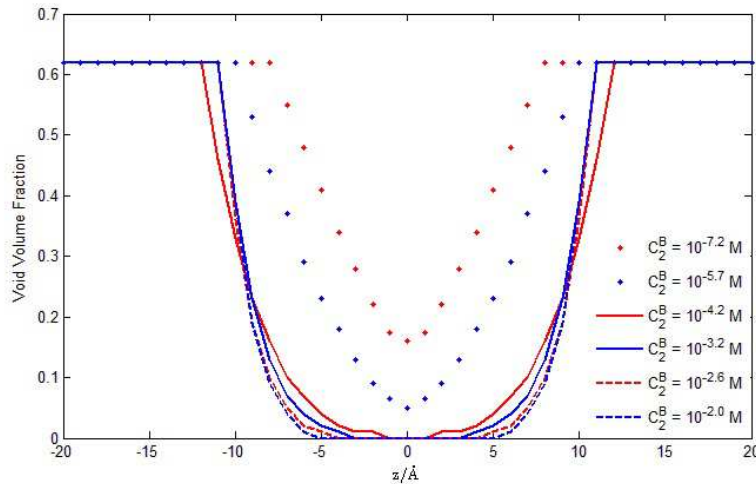


FIG. 8: The averaged void volume fraction $\Gamma(\mathbf{r})$ profiles.

11 also increases from 261.83 to 408.53 M in this range. The largest concentration is still below the maximum allowable value $C_2^{\text{Max}} = 1/v_2 = 408.57$ M as implied by the Fermi distribution (7). We obtained this incredibly large concentration since $O_2^b \approx 1$ in (19), which in turn yields $1/v_b \approx 408.53$ M as $v_b \approx v_2$ indicating the importance of the atomic nature of the steric potential (19) with variable v_b . This figure demonstrates that the PNPf model can capture the atomic properties of ions in flow, a critical (however small) step in continuum theory toward the ultimate accuracy in theoretical simulations. From Fig. 3, we observe that Ca^{2+} currents increase dramatically when $[\text{Ca}^{2+}]_o$ increases from $10^{-3.2}$ to 10^{-2} M in the physiological mM range of Ca_V channels. The corresponding flux density profiles in the binding region increase dramatically too as shown in Fig. 12.

We make a final remark about these results. As intensively studied in [37, 71, 72], the

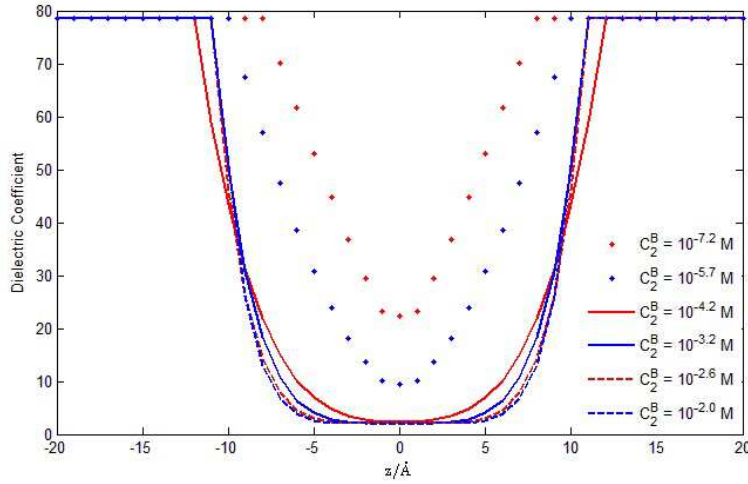


FIG. 9: The averaged dielectric function $\tilde{\epsilon}(\mathbf{r})$ profiles.

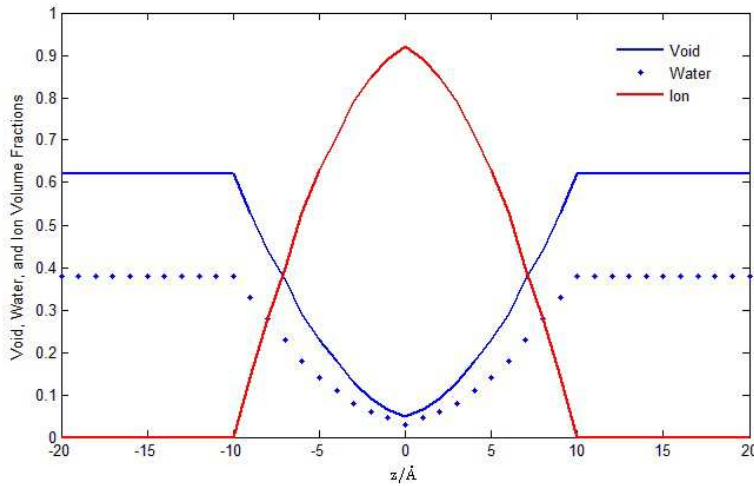


FIG. 10: Crowded Charge in Binding Site. The volume fractions of voids, water, and ions per unit volume at the Ca^{2+} bath concentration $C_2^{\text{B}} = 10^{-5.7}$ M.

classical PNP model fails to yield ionic concentrations and currents properly (compared with those of Brownian dynamics), especially for narrow channels, because the classical model does not include the volume effect of ions, water, and voids, the correlation effect of ions, and the screening effect of water. The PNPF model not only computes ionic currents comparable to the experimental data (Fig. 3) for the narrow calcium channel but also provides many physical properties (Figs. 5-10, for example) that are shown to depend critically on the proposed steric potential. The PNPF model overcomes the limitation of the classical PNP model with respect to these effects and properties.

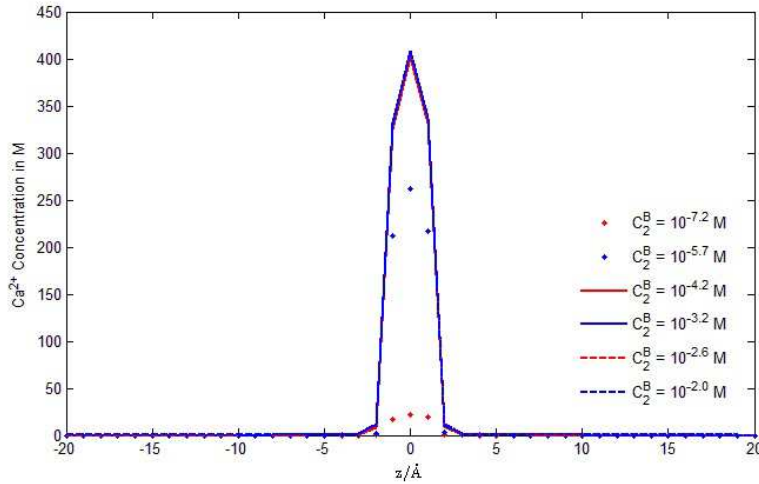


FIG. 11: The averaged Ca^{2+} concentration $C_2(\mathbf{r})$ profiles.

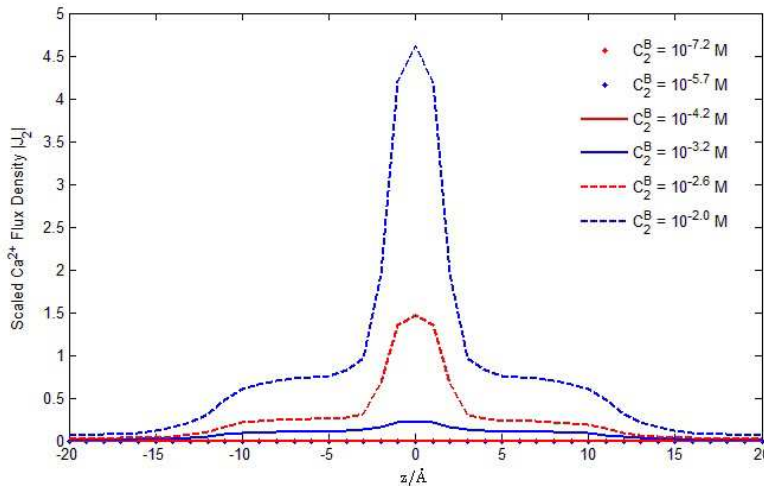


FIG. 12: The averaged Ca^{2+} flux density $|\mathbf{J}_2(\mathbf{r})|$ profiles.

6. CONCLUSION

We propose a Poisson-Nernst-Planck-Fermi model for studying equilibrium and nonequilibrium systems of ionic liquids and solution electrolytes. The excluded volume effect of different sizes of ions and water molecules, the correlation effect of crowded ions, and the screening effect of polar water molecules in inhomogeneous aqueous electrolytes are all included in this model. The model was verified by a set of experimental currents of L-type Ca channels recorded in a 10^8 -fold range of Ca^{2+} concentrations that show the exceptional selectivity of these channels.

We also propose a consistent Gibbs free energy functional leading to a Fermi like distribution of hard spherical particles in the electrolytic system. The Gibbs-Fermi functional

is shown to converge to the Gibbs-Boltzmann functional that yields the Boltzmann distribution as the volumes of all particles and the correlation length approach zero. Moreover, we introduce a Gibbs-Fermi entropy for which the excluded volume of water molecules and the dynamic distribution of interstitial voids between particles are needed to establish a consistent generalization of nonideal inhomogeneous electrolytes for both equilibrium and nonequilibrium systems. The local probability of any particle species in the Gibbs-Fermi entropy is expressed in terms of the local and bulk ratios between the particle and void fractions per unit volume. We show that if all particles are treated as hard spheres, the voids must be included in the Gibbs free energy functional. The voids are created by packing defects and Lennard-Jones and Coulomb forces between particles. The void effect plays an essential role in our theory as well as in our results, especially in the steric energy.

Most of the results in this article seem to be novel, because consistent models including voids, water volume, and Fermi distributions have not been developed previously, as far as we know. These numerical results provide useful tools to develop insight into a variety of physical mechanisms ranging from binding, to permeation, blocking, flexibility, and charge/space competition of the channel.

Acknowledgments

This work was supported in part by National Science Council of Taiwan under Grant No. 102-2115-M-134-005 to J.L.L. and by the Bard Endowed Chair of Rush University Medical Center, held by B.E.

-
- [1] B. Eisenberg, *Biophys. J.* **104**, 1849 (2013).
 - [2] W. Almers and E. W. McCleskey, *J. Physiol.* **353**, 585 (1984).
 - [3] D. D. Friel and R. W. Tsien, *Proc. Natl. Acad. Sci.* **86**, 5207 (1989).
 - [4] A. Rodriguez-Contreras, W. Nonner, and E. N. Yamoah, *J. Physiol.* **538**, 729 (2002).
 - [5] W. A. Sather and E. W. McCleskey, *Annu. Rev. Physiol.* **65**, 133 (2003).
 - [6] L. Tang, T. M. G. El-Din, J. Payandeh, G. Q. Martinez, T. M. Heard, T. Scheuer, N. Zheng, W. A. Catterall, *Nature* **505**, 56 (2014).
 - [7] A. L. Hodgkin, *Biol. Rev. Camb. Philos. Soc.* **26**, 339 (1951).
 - [8] B. Hille, *Ionic Channels of Excitable Membranes*, (Sinauer Associates Inc., Sunderland, MA 2001).
 - [9] D. P. Chen, V. Barcion, and R. S. Eisenberg, *Biophys. J.* **61**, 1372 (1992).
 - [10] R. Eisenberg and D. Chen, *Biophys. J.* **64**, A22 (1993).
 - [11] R. S. Eisenberg, M. M. Kłosek, and Z. Schuss, *J. Chem. Phys.* **102**, 1767 (1995).
 - [12] J.-L. Liu and B. Eisenberg, *J. Phys. Chem. B* **117**, 12051 (2013).
 - [13] J.-L. Liu, *J. Comp. Phys.* **247**, 88 (2013).
 - [14] J.-L. Liu and B. Eisenberg, *J. Chem. Phys.* **141**, 075102 (2014).
 - [15] D. Boda, M. Valiskó, B. Eisenberg, W. Nonner, D. Henderson, and D. Gillespie, *Phys. Rev. Lett.* **98**, 168102 (2007).
 - [16] D. Gillespie and D. Boda, *Biophys. J.* **95**, 2658 (2008).
 - [17] D. Boda, M. Valiskó, D. Henderson, B. Eisenberg, D. Gillespie, and W. Nonner, *J. Gen. Physiol.* **133**, 497 (2009).

- [18] A. Malasics, D. Gillespie, W. Nonner, D. Henderson, B. Eisenberg, and D. Boda, *Biochim. Biophys. Acta* **1788**, 2471 (2009).
- [19] D. Boda, D. Henderson, and D. D. Busath, *J. Phys. Chem. B* **105**, 11574 (2001).
- [20] D. Boda, D. D. Busath, B. Eisenberg, D. Henderson, and W. Nonner, *Phys. Chem. Chem. Phys.* **4**, 5154 (2002).
- [21] D. Gillespie, L. Xu, Y. Wang, and G. Meissner, *J. Phys. Chem. B* **109**, 15598 (2005).
- [22] J. Giri, J. E. Fonseca, D. Boda, D. Henderson, and B. Eisenberg, *Phys. Biol.* **8**, 026004 (2011).
- [23] H. Alle, A. Roth, and J. R. P. Geiger, *Science* **325**, 1405 (2009).
- [24] P. J. Magistretti, *Science* **325**, 1349 (2009).
- [25] C. A. Kraus, *Bull. Amer. Math. Soc.* **44**, 361 (1938).
- [26] J. F. Zemaitis Jr., D. M. Clark, M. Rafal, and N. C. Scrivner, *Handbook of Aqueous Electrolyte Thermodynamics* (Design Institute for Physical Property Data, American Institute of Chemical Engineers, New York, 1986).
- [27] K. S. Pitzer, *Thermodynamics* (McGraw Hill, New York, 1995).
- [28] R. T. Jacobsen, S. G. Penoncello, E. W. Lemmon, and R. Span, in *Multiparameter Equations of State. Equations of State for Fluids and Fluid Mixtures*, edited by J. V. Sengers, R. F. Kayser, C. J. Peters and H. J. White, Jr., 849-882 (Elsevier, New York 2000).
- [29] K. J. Laidler, J. H. Meiser, and B. C. Sanctuary, *Physical Chemistry* (Brooks Cole, Belmont, CA, 2003).
- [30] W. R. Fawcett, *Liquids, Solutions, and Interfaces: From Classical Macroscopic Descriptions to Modern Microscopic Details* (Oxford University Press, New York, 2004).
- [31] Y. Lin, K. Thomen and J.-C. de Hemptinne, *AIChE J.* **53**, 989 (2007).
- [32] G. Lebon, D. Jou, and J. Casas-Vázquez, *Understanding Non-equilibrium Thermodynamics: Foundations, Applications, Frontiers* (Springer, 2008).
- [33] G. M. Kontogeorgis and G. K. Folas, *Thermodynamic Models for Industrial Applications: From Classical and Advanced Mixing Rules to Association Theories* (John Wiley & Sons, 2009).
- [34] P. Hünenberger and M. Reif, *Single-ion Solvation. Experimental and theoretical approaches to elusive thermodynamic quantities* (Royal Society of Chemistry, London 2011).
- [35] G. M. Lipkind and H. A. Fozzard, *Biochem.* **40**, 6786 (2001).
- [36] G. Barreiro, C. R. Guimaraes, and R. B. de Alencastro, *Protein Eng.* **15**, 109 (2002).
- [37] B. Corry, S. Kuyucak, and S.-H. Chung, *Biophys. J.* **78**, 2364 (2000).
- [38] B. Corry, T. W. Allen, S. Kuyucak, and S.-H. Chung, *Biophys. J.* **80**, 195 (2001).
- [39] I. Kaufman, D. G. Luchinsky, R. Tindjong, P. V. E. McClintock, and R. S. Eisenberg, *Phys. Biol.* **10**, 026007 (2013).
- [40] D. Boda, D. D. Busath, D. Henderson, and S. Sokolowski, *J. Phys. Chem. B* **104**, 8903 (2000).
- [41] T.-L. Horng, T.-C. Lin, C. Liu, and B. Eisenberg, *J. Phys. Chem. B* **116**, 11422 (2012).
- [42] W. Nonner and B. Eisenberg, *Biophys. J.* **75**, 1287 (1998).
- [43] W. Nonner, L. Catacuzzeno, and B. Eisenberg, *Biophys. J.* **79**, 1976 (2000).
- [44] W. Nonner, D. Gillespie, D. Henderson, and B. Eisenberg, *J. Phys. Chem. B* **105**, 6427 (2001).
- [45] C. N. Schutz, A. Warshel, *Proteins* **55**, 711 (2004).
- [46] G. R. Desiraju, T. Steiner, *The Weak Hydrogen Bond: In Structural Chemistry and Biology* (Oxford, 2001).
- [47] Z. Schuss, *Theory and Applications of Stochastic Processes: An Analytical Approach* (Springer, New York, 2009).
- [48] Z. Schuss, B. Nadler, and R. S. Eisenberg, *Phys. Rev. E* **64**, 036116 (2001).

- [49] A. Singer, Z. Schuss, B. Nadler, and R. S. Eisenberg, Proc. SPIE **5467**, 345 (2004).
- [50] M. Z. Bazant, Acc. Chem. Res. **46** (2013) 1144.
- [51] R. S. Eisenberg, J. Membr. Biol. **150**, 1 (1996).
- [52] A. L. Hodgkin, A. F. Huxley, and B. Katz, Arch. Sci. Physiol. **3**, 129 (1949).
- [53] F. Bezanilla, Physiol. Rev. **80**, 555 (2000).
- [54] F. Bezanilla and C. A. Villalba-Galea, J. Gen. Physiol. **142**, 575 (2013).
- [55] D. A. McQuarrie, *Statistical Mechanics* (Harper and Row, New York, 1976).
- [56] C. D. Santangelo, Phys. Rev. E **73**, 041512 (2006).
- [57] M. Z. Bazant, B. D. Storey, and A. A. Kornyshev, Phys. Rev. Lett. **106**, 046102 (2011).
- [58] G.-W. Wei, Q. Zheng, Z. Chen, K. Xia, SIAM Rev. **54**, 699 (2012).
- [59] I. Borukhov, D. Andelman, and H. Orland, Phys. Rev. Lett. **79**, 435 (1997).
- [60] B. Li, SIAM J. Math. Anal. **40**, 2536 (2009).
- [61] A. R. J. Silalahi, A. H. Boschitsch, R. C. Harris, and M. O. Fenley, J. Chem. Theory Comput. **6**, 3631 (2010).
- [62] B. Lu and Y. C. Zhou, Biophys. J. **100**, 2475 (2011).
- [63] S. Zhou, Z. Wang, and B. Li, Phys. Rev. E **84**, 021901 (2011).
- [64] Y. Qiao, B. Tu, and B. Lu, J. Chem. Phys. **140**, 174102 (2014).
- [65] L. Verlet, Phys. Rev. **159**, 98 (1967).
- [66] B. Eisenberg, Y. Hyon, and C. Liu, J. Chem. Phys. **133**, 104104 (2010).
- [67] D. Boda, W. R. Fawcett, D. Henderson, and S. Sokolowski, J. Chem. Phys. **116**, 7170 (2002).
- [68] J. Liao, H. Li, W. Zeng, D. B. Sauer, R. Belmares, and Y. Jiang, Science **335**, 686 (2012).
- [69] M. Liao, E. Cao, D. Julius, and Y. Cheng, Nature **504**, 107 (2013).
- [70] M. G. Kurnikova, R. D. Coalson, P. Graf, and A. Nitzan, Biophys. J. **76**, 642 (1999).
- [71] W. Im, B. Roux, Biophys. J. **115**, 4850 (2001).
- [72] W. Im and B. Roux, J. Mol. Biol. **322**, 851 (2002).
- [73] B. Eisenberg, J. Phys. Chem. C **114**, 20719 (2010).
- [74] D. Boda, W. Nonner, D. Henderson, B. Eisenberg, and D. Gillespie, Biophys. J. **94**, 3486 (2008).
- [75] B. Lu and J. A. McCammon, Chem Phys Lett. **451**, 282 (2008).